Available online at www.sciencedirect.com

ScienceDirect

Energy Procedia 00 (2018) 000–000

Energy Procedia

www.elsevier.com/locate/procedia

73rd Conference of the Italian Thermal Machines Engineering Association (ATI 2018), 12-14 September 2018, Pisa, Italy

Numerical modelling and experimental validation of jet impingement technology for professional appliances

Emidio Tiberi[a,b,*], Riccardo Furlanetto[b], Michele Simonato[b], Marzio Piller[a]

[a]*Dipartimento di Ingegneria e Architettura, Università degli Studi di Trieste, Via A. Valerio 10, 34127 Trieste, Italy*
[b]*The Research Hub[TM] by Electrolux Professional, Viale Treviso 15, 33170 Pordenone, Italy*

Abstract

We propose a combined numerical/experimental investigation of the heating/cooling process taking place in modern jet-impingement (JI henceforth) professional appliances. In food processing, the JI is mainly employed in industrial continuous *tunnel* machines, though it is exploited also in some professional appliances operating in batch mode. We set up an experimental facility, representative of a typical commercial JI appliance for food processing, in terms of dimensions and operative conditions. Experiments are carried out to provide the spatial distribution of the heat transfer coefficient on the exposed surface of a thick metal slab, positioned at known distance from the nozzles, under cooling conditions. Velocity and temperature measurements are acquired and compared against the numerical results. Once validated, the proposed numerical model can provide detailed maps of the Nusselt number under different flow conditions. These, in turn, are used as input data for a computationally-efficient, numerical heat-conduction model, which can be envisaged as a potential design tool for heating/cooling professional appliances based on JI technology.

Keywords: jet impingement; cooling process; 3D conduction model; validation; experimental test rig; design tool; high speed professional appliance.

1. Introduction

Jet impingement is an efficient heat and mass transfer technology, where a high-speed airflow is directed towards an object from a single nozzle or an array of nozzles, resulting in high heat and mass transfer coefficients on the impinged surface. This technology is widely used food processing industry, both for industrial *tunnel* machines that work mainly in continuous mode [14] and professional appliances that work mainly in batch mode [15]. The proposed investigation

*Corresponding author. Tel.: +39-3480666856.
E-mail address: emidio.tiberi@phd.units.it

aims to devise and validate a usable, flexible and brisk design tool for professional food-treatment appliance exploiting the JI technology. The proposed tool can be used to optimize the heating/cooling time and the temperature distribution inside treated food items without affecting the final quality of the products. Indeed it is well known that rapid cooling methods prevent the growth of microorganisms and reduce the evaporative weight losses, resulting in improved food quality ([12],[13]). Several studies focus on the impingement technology for food processing. Erdogdu et al. [6] develop a mathematical model to simulate the cooling process of a finite slab shaped object using a single air jet and measure the spatial variation of the convective heat transfer coefficient over the surface. A two layer material is studied, to mimic the behaviour of heterogeneous food. The numerical predictions and the experimental results are in excellent agreement, provided the spatial variation of the heat-transfer coefficient is accounted for. Erdogdu et al. [7] study the effects of the impingement technology on the cooling of boiled eggs, as an alternative procedure to water immersion. A numerical model is proposed and validated against experimental data. Anderson et al. [9] propose a method to study the impingement technology for thawing processes of frozen food: they develop an inverse method to estimate the spatial distribution of the heat transfer coefficient during the thawing process of a tylose disk (typically used to reproduce the thermal behaviour of meat [11]); the procedure becomes inaccurate when the temperature difference between air and the surface drops below 1 °C.

The proposed research focuses on the transient thermal behaviour of an object under an array of jets in a confined domain representative of a cavity of a commercial professional appliance. A numerical model is used to calculate the distribution of the Nusselt number on the surface of the object: the resulting maps are used as boundary condition in a finite-difference conductive numerical model. The predicted temperatures are compared with experimental data for a thick metal slab.

Nomenclature

T	Temperature $[K]$	H	Nozzle-to-surface distance $[m]$
$\overline{q''}$	Heat flux $[W/m^2]$	λ	Thermal conductivity $[W/mK]$
x,y,z	Cartesian coordinates $[m]$	ρ	Density $[kg/m^3]$
t	Time $[s]$	c	Specific heat $[J/kgK]$
α	Thermal diffusivity $[m^2/s]$	Nu	Nusselt number
h	Convective heat transfer coefficient $[W/m^2K]$	Re	Reynolds number
D	Nozzle diameter $[m]$		
Subscripts		∞	Nozzle outlet conditions
w	Wall conditions	0	Initial conditions

2. Materials and methods

2.1. Test rig

The experimental facility, shown in figure 1a, consists of a closed loop air circuit endowed with a centrifugal blower, whose rotational speed is controlled by an inverter to attain a prescribed airflow rate, as measured by a calibrated orifice. The device operates either in cooling or heating modes: to this end, the airflow goes through two independent heat exchangers before entering the test chamber. A plenum is placed upstream the array of nozzles to provide a uniform pressure further up the array of nozzles and the detachable nozzle plate permits the study of different nozzle geometries (the nozzle system is sketched in figure 1b). The exhaust air is collected below the test chamber and then recirculated to the blowing system. The thermodynamic conditions inside the test chamber are controlled by the heating/cooling elements (ON/OFF control strategy with dead-band). Inside the test chamber a shelf can be moved

vertically to study different nozzle-to-plate distances. For all the experiments the temperature of the laboratory is kept between 20 °C and 25 °C with a relative humidity between 50% and 60 %.

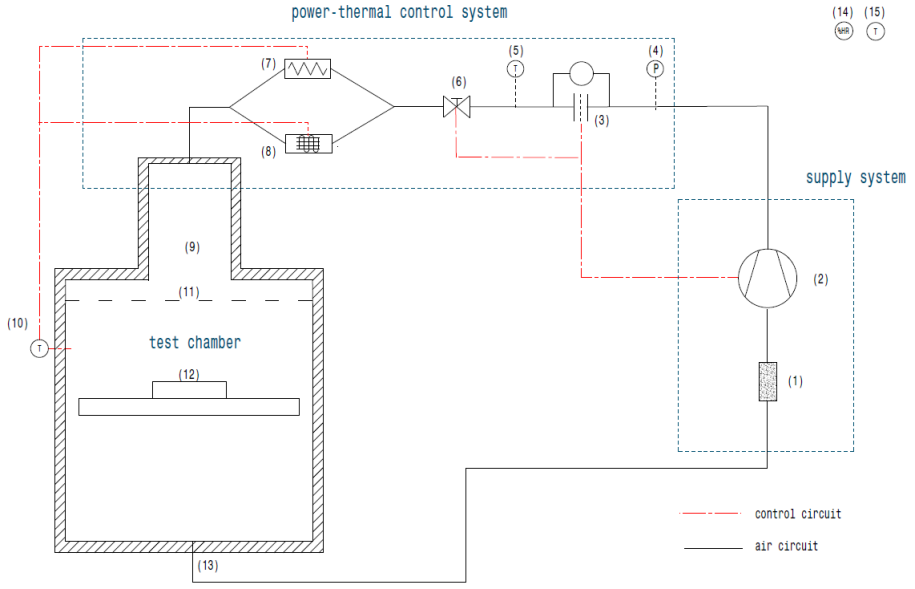

(a) Test rig scheme: 1) air filter, 2) blower, 3) volumetric flow meter, 4) pressure gauge, 5) temperature transducer, 6) throttling valve, 7) heaters, 8) chiller, 9) plenum, 10) temperature transducer, 11) nozzles plate, 12) target, 13) recirculating duct.

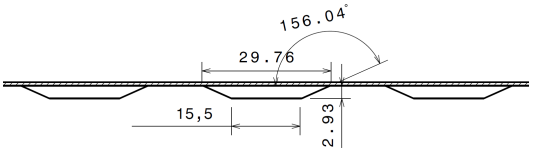

(b) The geometry of the nozzles (dimensions in mm)

Fig. 1: Experimental facility

The time rate-of-change of the temperature is measured on the surface of a thick metal slab cooled by the jets. The sizes of the slab are 300 mm in length, 300 mm in width and 5 mm in thickness. It is made of AISI 304 stainless steel ($\lambda = 17\,W/mK$, $\rho = 7800\,kg/m^3$ and $c = 480\,J/kgK$). Eleven thermocouples are welded on the bottom of the plate as shown in figure 2: those marked in red are exactly at the stagnation points, the others are placed halfway between neighbouring stagnation points (hereinafter indicated as *intermediate* zones). T-type thermocouples (36 gauge) are used with ±1°C accuracy in the range -200 °C / 350 °C. The metal slab is heated up to 65 °C by means of a heating module made of a resistor, annealed in a block of aluminium to provide a uniform heat flux. After reaching the set point the heating module is swiftly removed and the blower is activated. Two different Reynolds numbers (16000 and 21000) are studied with a nozzle-to-plate dimensionless distance (H/D) of 5.

2.2. Numerical CFD model

The commercial CFD (Computational Fluid Dynamics) solver STARCCM+® is used to solve the thermofluid-dynamic field inside the test chamber and to provide the distribution of the Nusselt number on the surface of the plate. The computational domain, shown in figure 3a, corresponds to the test chamber and is discretized by an unstructured polyhedral mesh with about two millions cells. The mesh size is refined in the jet and free-jet zones (1,5 mm as characteristic length), in the zones near the wall (1,2 mm as characteristic length) and at the wall with 10 layers

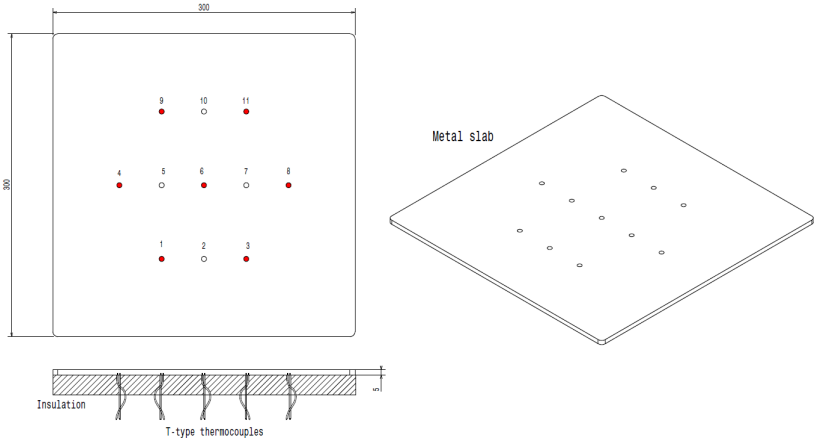

Fig. 2: Metal slab assembly: the thermocouples in red are exactly at the stagnation points

of prisms with a total thickness of 0,7 mm (figures 3b and 3c). A mesh-refinement study, not reported for brevity, shows that further refinements of the considered mesh do not yield significant improvements of the results. Mass-flow inlet boundary conditions are prescribed on an a horizontal plane positioned in the plenum region, in order to ensure a uniform velocity profile. A constant, uniform pressure is enforced at the outlets, where the airflow leaves the test chamber. The fluid domain is confined by the walls of the test chamber, considered adiabatic. The plate is treated as solid medium that interacts with the fluid by transient conjugate heat transfer. As initial condition we assume that the air in the whole chamber is at rest and at uniform temperature of 25 °C and that the plate has a uniform temperature of 65 °C. The governing equations for the turbulence are solved by the RANS SST $k - \omega$ model, suitable for flows with adverse pressure gradient and high wall gradients, as impinging jets [5].

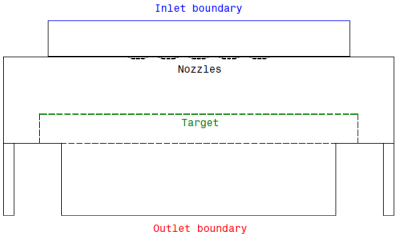

(a) Sketch of the computational domain.

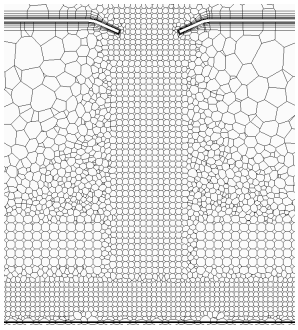

(b) Mesh

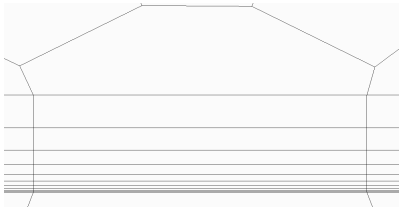

(c) Prism layer mesh

Fig. 3: Geometry and mesh

The SIMPLE algorithm is adopted to solve the pressure-velocity coupling and the convective scheme is Upwind 2nd order accurate, with the *low-Re number* method for the wall treatment [8]. The target is a slab of AISI 304 stainless steel with constant thermal properties and the fluid is air with ideal gas properties. The fluid is considered incompressible since no differences emerge when the buoyancy term is considered in the model.

2.3. Heat transfer coefficients

The distribution of the heat transfer coefficient (or Nusselt number, defined in (1)) on the target surface is derived by numerical simulation and measured experimentally by micro-calorimeters [1, 10], consisting of small copper disks

(5 mm diameter). The disks are firstly heated by an external device and then cooled by the air flow delivered from the nozzles. Each disk is modelled by the lumped-capacitance approach (Biot number less than 0.01) and therefore its temperature during the cooling process can be used to calculate the local heat transfer coefficient as suggested by [10]. The numerical and experimental distributions of the Nusselt number on the target surface are reported in figure 4 and 5 for two Reynolds numbers, defined by the diameter of the nozzle and the airflow velocity at the exit of the nozzle: for both Reynolds numbers, the average relative error between numerical and experimental results is about 20%. This value is considered acceptable and in line with the uncertainty of the measurement technique of heat transfer coefficients with transient methods (the typical range of error reported in literature is from 10% to 15% at 95% of confidence level [1]). The error can be related to several factors, from the change in weight and shape of each copper disk after the welding process of the thermocouples to the presence of insulating material used to isolate laterally each copper disk and create the lumped system (on the contrary, in the simulation the plate is considered uniform). The time-dependent numerical simulation allows to study in detail the evolution of the Nusselt number: the temporal evolution of Nu is characterized by a steep rise, gradually settling on a stationary value, as found by other researchers [3]. Once reached the Nu stabilization, a brief interval, equal to 4-5 times the residence time of the fluid within the test chamber, has been considered for the evaluation of the local Nu number.

$$Nu = \frac{hD}{\lambda} = \frac{\overline{q''}D}{\lambda(T_\infty - T_w)} \tag{1}$$

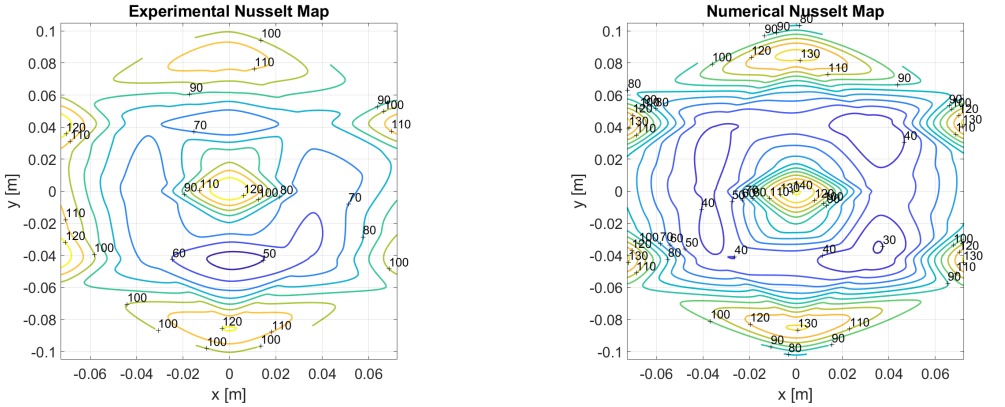

Fig. 4: Nusselt maps for Re=16000

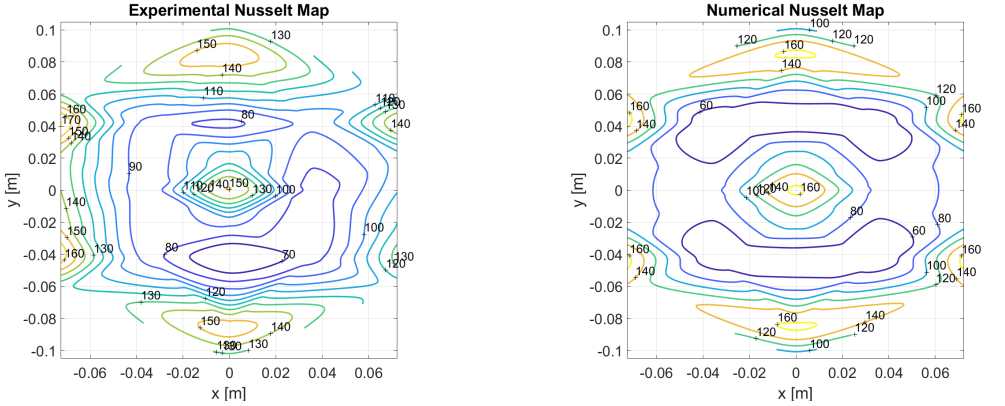

Fig. 5: Nusselt maps for Re=21000

2.4. Finite difference 3D model

A finite difference 3D model has been implemented in MATLAB® to solve the heat conduction equation inside the metal slab. The mathematical model for three-dimensional, unsteady heat conduction throughout a homogeneous, isotropic solid is:

$$\begin{aligned}
&\frac{\partial^2 T}{\partial x^2} + \frac{\partial^2 T}{\partial y^2} + \frac{\partial^2 T}{\partial z^2} = \frac{1}{\alpha}\frac{\partial T}{\partial t} \\
&-\lambda \frac{\partial T}{\partial x}\Big|_{x=x_{min}} = 0 \qquad -\lambda \frac{\partial T}{\partial x}\Big|_{x=x_{max}} = 0 \qquad -\lambda \frac{\partial T}{\partial y}\Big|_{y=y_{min}} = 0 \qquad -\lambda \frac{\partial T}{\partial y}\Big|_{y=y_{max}} = 0 \\
&-\lambda \frac{\partial T}{\partial z}\Big|_{z=z_{bottom}} = 0 \qquad -\lambda \frac{\partial T}{\partial z}\Big|_{z=z_{top}} = h(x,y)[T(x,y,z_{top},t) - T_\infty(t)] \\
&T(x,y,z,0) = T_0
\end{aligned} \tag{2}$$

A 3-D first order explicit finite difference model has been implemented [2]; the timestep is set accordingly to the stability criterion $\frac{\alpha \Delta t}{\Delta z^2} \leq \frac{1}{2}$, where Δz is the minimum spatial difference between the nodes of the mesh. On the top surface the convective boundary condition is used: the spatial variation of h-value is retrieved from the whole map of coefficients (as in figure 6) by interpolating the local values. The other boundaries are considered adiabatic. The boundary condition on the top surface takes into account only the convection coefficient, as the radiation heat transfer between the slab and the surrounding is negligible due to the low temperature difference: the initial condition of the slab is 65 °C and the chamber is at 27 °C. In this condition the radiative heat transfer coefficient can be estimated as 7.4 W/m^2K (approximating the slab as a small, black surface placed within a large cavity) and this value decreases over time during the cooling process of the slab.

3. Results and discussion

A transient, three-dimensional model is used to simulated the conjugate heat transfer between a thick metal plate and the airflow issued from an array of nozzles. The resulting distribution of the Nusselt number on the surface of the plate is used as boundary condition for a transient, three-dimensional heat conduction model.

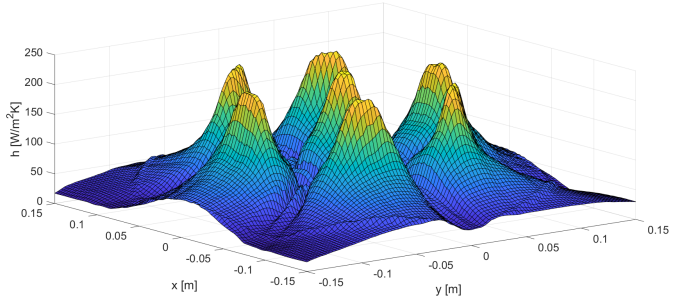

Fig. 6: Map of heat transfer coefficients for Re=16000

The numerical temperature profiles at the given locations (figure 2) are compared with the experimental results and a good agreement is found for all the considered conditions (figure 7). The experimental data are chosen by averaging the results of three tests, carried out for both Reynolds numbers 16000 and 21000. It is evident in figure 7 that the spatial distribution of the h-values affects the thermal behaviour of the slab. Indeed at the stagnation points the cooling rate is higher than at different locations as expected. This consideration is confirmed also studying the effect of a constant heat transfer coefficient on the top surface. In literature several semi-empirical correlations have been

developed to describe the jet impingement heat transfer mechanism [4, 5]: for array of jets the correlations provide the average Nusselt number on the target surface.

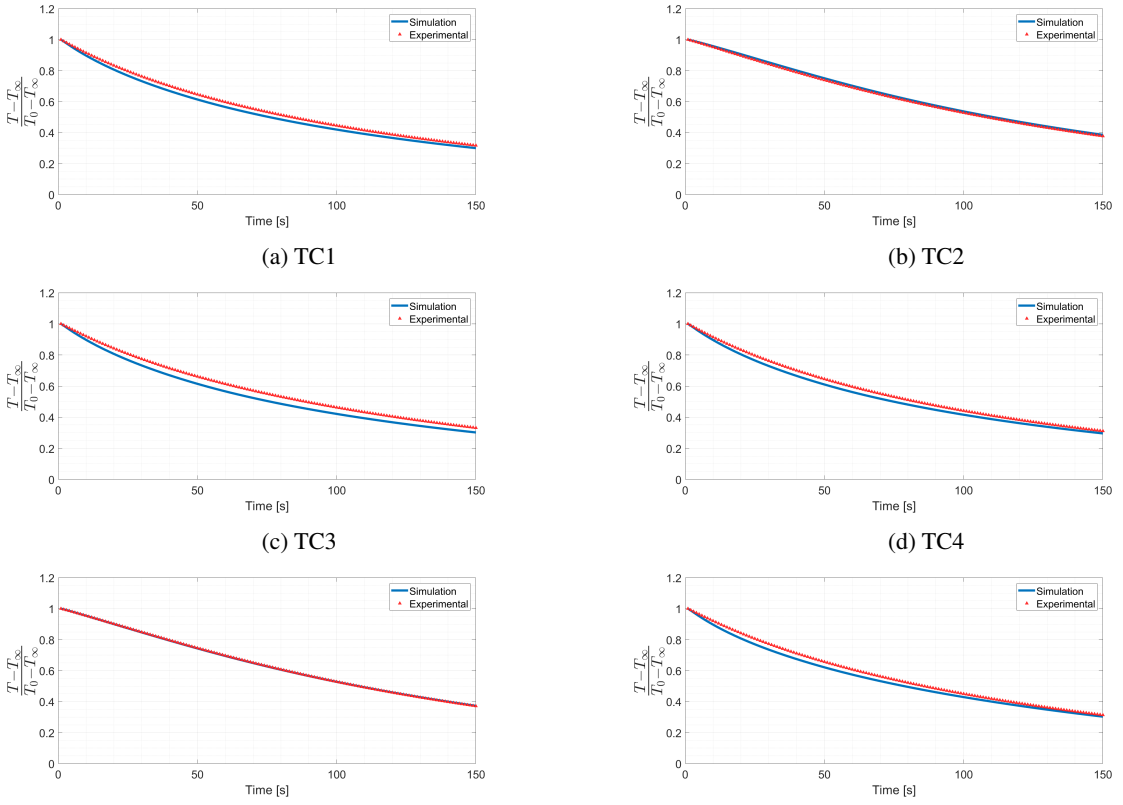

(a) TC1 (b) TC2

(c) TC3 (d) TC4

(e) TC5 (f) TC6

Fig. 7: Comparison between experimental and numerical predicted results for Re=21000

In figure 8 three different boundary conditions on the top surface are compared: respectively the detailed spatial distribution provided by CFD, the average value of the distribution ($\bar{h}_{CFD}$ hereinafter) and a h-value obtained by semi-empirical correlations [4] ($\bar{h}_{Martin}$ hereinafter).

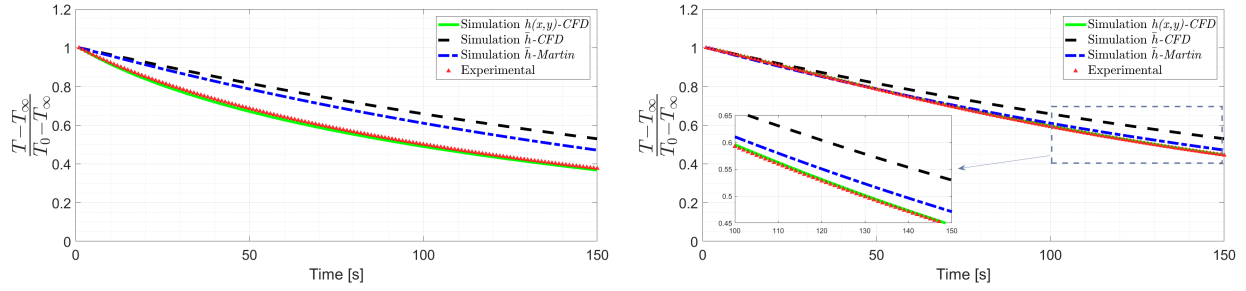

(a) Stagnation zone (b) Intermediate zone

Fig. 8: Effect of spatial variation of Nusselt number for Re=16000

The two graphs in figure 8 are referred respectively to a stagnation point (TC9) and an intermediate point (TC5). Firstly it appears evident that both $\bar{h}_{CFD}$ and $\bar{h}_{Martin}$ boundary conditions slow down remarkably the cooling process

nearby the stagnation region, while the effect is substantially reduced in the intermediate zone. This effect is particularly evident because the average operation tends to penalize much more the zones in which there are peaks of Nusselt number. The Martin's correlation results in a higher value of heat transfer coefficient (90 W/m^2K) than the one averaged from the distribution (80 W/m^2K), since it considers an infinite array of jets and it does not take into account the border effects. By chance, it turns out that it yields better accuracy for the intermediate points which are far enough from the boundaries.

4. Conclusions

Jet impingement can be considered a promising heat transfer technology for food processing applications. Advanced design tools, as numerical simulation, are needed to capture all the relevant phenomena that govern this heat transfer process. We propose and validate a reliable and computationally efficient numerical design tool. A CFD model is implemented to study the thermofluid-dynamic behaviour of the system and obtain the maps of the Nusselt number on the impinged target. These maps are validated with experimental data obtained with the micro-calorimeters technique. The maps are then imported into a finite-difference heat-conduction model that simulates the temperature field within the object: a remarkably good agreement is found with experimental temperature data for a thick metal slab. The spatial distribution of the heat transfer convective coefficient has a significant impact on the time rate of change of the temperature: assuming a uniform distribution of the h-value causes a significant underestimate of the cooling rate of the object placed beneath the jets.

References

[1] Sarkar, A. and Singh, R.P., "Spatial variation of convective heat transfer coefficient in air impingement applications", *Journal of Food Science* 68(3) (2003): 910-916.
[2] Chau, K.V. and Gafney, J.J., "A finite difference model for heat and mass transfer in products with internal heat generation and transpiration", *Journal of Food Science* 55 (1990): 484-487.
[3] Kim, K. and Camci, C., "Fluid dynamics and convective heat transfer in impinging jets through implementation of a high resolution liquid crystal technique", *International Journal of Turbo and Jet Engines* 12 (1995): 1-12.
[4] Martin, H., "Heat and Mass Transfer between Impinging Gas Jets and Solid Surfaces", *Advances in Heat Transfer* 13 (1977): 1-60.
[5] Zuckerman, N. and Lior, N., "Jet Impingement Heat Transfer: Physics, Correlations, and Numerical Modeling", *Advances in Heat Transfer* 39 (2006): 565-631.
[6] Erdogdu, F., Sarkar, A. and Singh, R.P., "Mathematical modeling of air-impingement cooling of finite slab shaped objects and effect of spatial variation of heat transfer coefficient", *Journal of Food Engineering* 71 (2005): 287-294.
[7] Erdogdu, F., Ferrua, M., Singh, S. and Singh, R.P., "Air impingement cooling of boiled eggs: Analysis of flow visualization and heat transfer", *Journal of Food Engineering* 79 (2007): 920-928.
[8] Pope, S.B., *Turbulent Flows*, (2000) Cambridge University Press
[9] Anderson, B.A. and Singh, R.P., "Effective heat transfer coefficient measurement during air impingement thawing using an inverse method", *International Journal of Refrigeration* 29 (2006): 281-293.
[10] Donaldson, C.D., Snedeker, R.S. and Margolis, D.P., "A study of free jet impingement. Part 2. Free jet turbulent structure and impingement heat transfer", *Journal of Fluid Mechanics* 45(3) (1971): 477-512.
[11] Anderson, B.A. and Singh, R.P., "Moisture diffusivity in tylose gel", *Journal of food science* 70(5) (2005): 331-337.
[12] Ketteringham, L. and James, S., "The use of high thermal conductivity inserts to improve the cooling of cooked foods", *Journal of food engineering* 45 (2000): 49-53.
[13] Landfeld, A., Houska, M., Kyhos, K. and Jiang-Qibin, "Mass transfer experiments on vacuum cooling of selected pre-cooked solid foods", *Journal of food engineering* 52 (2002): 207-210.
[14] GEA Group, "GEA HVF-series impingement freezer", *Technical Brochure*, [online access 18/05/2018], https://www.gea.com/it/products/gea-hvf-series-impingement-freezers.jsp.
[15] Merrychef, "Eikon® e2s", *Technical Brochure*, [online access 18/05/2018], http://www.merrychef.com/Product/fam_rtdfja/eikon-e2s#downloads.